Electromagnetic-Force-Induced Convection in Weld Pools with a Free Surface

A model is developed to predict heat transfer, fluid flow and pool shape in GTAW

BY M. C. TSAI AND S. KOU

ABSTRACT. Electromagnetic-force-induced convection in the weld pool during gas tungsten arc welding was studied, the shape of the weld pool surface being unknown. In order to accurately describe the boundary conditions, pool-surface fitting orthogonal curvilinear coordinates were used. The current density, the self-induced magnetic field and the resultant electromagnetic force in the weld pool were calculated. Based on the electromagnetic-force distribution, heat transfer and fluid flow in the weld pool and the shape of the pool surface were calculated and discussed. In order to check the validity of the model, the calculated pool surface deformation due to a point current source was compared with the theoretical analysis of Sozou.

Introduction

In view of the significant effect of weld pool convection on the microstructure and properties of the resultant weld, numerous investigators have attempted to calculate heat transfer and fluid flow in the weld pool. Most of these investigators have used either the rigid-lid assumption (Refs. 1–17) or the stepwise approximation (Refs. 18–20) for the weld pool surface. In the former, the pool surface was assumed flat and undeformable, while in the latter, the deformed pool surface was approximated by small steps of the finite difference grid closest to the pool surface.

Recently, McLay, *et al.* (Ref. 21), used the finite element method to calculate heat transfer and fluid flow in a weld pool. The shapes of the deformed pool surface and the pool bottom, which were specified rather than calculated, were closely fitted by finite element grids. Tsai, *et al.* (Refs. 22–24), on the other hand, used the finite difference method and pool-surface fitting orthogonal curvilinear coordinates to calculate the pool surface shape, as well as heat transfer and fluid flow in the weld pool. To allow examination of their individual effects on the deformation of the weld pool surface, the driving forces for convection/deformation, *i.e.,* the arc pressure, the surface tension gradient and density variations, were separated and studied individually. This study focuses on the effect of a different driving force, *i.e.,* the electromagnetic force, on pool surface deformation.

M. C. TSAI and S. KOU are with the Department of Materials Science and Engineering, University of Wisconsin, Madison, Wis.

Mathematical Formulation and Method of Solution

A schematic sketch of the physical system is shown in Fig. 1. As shown, the free surface is the surface of the weld pool, while the pool boundary is the liquidus isotherm T_L in the case of an alloy (as in the case of 6061 aluminum alloy in the present study) or the melting point T_m in the case of a pure metal. The distribution curve J represents the distribution of the welding current over the weld pool surface. For a Gaussian current density distribution over a flat pool surface,

$$J = \frac{3I}{\pi b^2} \exp\left(\frac{-3r^2}{b^2}\right) \quad (1)$$

where J is the current density, r the radial distance, I the welding current, and b the effective radius of the current density distribution, *i.e.,* J drops to 5% of its maximum value of $3I/\pi b^2$ at r = b.

Since the electrical conductivity is essentially constant in the workpiece metal, the distribution of the electric potential ϕ in the workpiece is described, in cylindrical coordinates r and z, by the following Laplace equation:

$$\frac{1}{r}\frac{\partial}{\partial r}\left(r\frac{\partial\phi}{\partial r}\right) + \frac{\partial^2\phi}{\partial z^2} = 0 \quad (2)$$

For a thick workpiece, which is effectively semi-infinite, the analytical solution to Equation (2), subjected to the boundary condition described in Equation (1), is as follows:

$$\phi(r,z) = \frac{I}{2\pi\sigma} \exp \int_0^\infty \left(-\frac{\lambda^2 b^2}{12}\right) \exp(-\lambda z)\, J_0(\lambda r)\, d\lambda \quad (3)$$

where σ is the electrical conductivity, J_0 the Bessel function of the zero order, and λ a dummy variable. The electrical conductivity σ is defined by the following Ohm's law:

$$\vec{J} = -\sigma\nabla\phi \quad (4)$$

For a deformed pool surface, however, the distribution of the electric potential ϕ in the workpiece is described, in axisymmetric orthogonal curvilinear coordinates η and ξ, by the following equation:

$$\frac{1}{h_1 h_2 r}\left[\frac{\partial}{\partial\eta}\left(\frac{h_2 r}{h_1}\frac{\partial\phi}{\partial\eta}\right) + \frac{\partial}{\partial\xi}\left(\frac{h_1 r}{h_2}\frac{\partial\phi}{\partial\xi}\right)\right] = 0 \quad (5)$$

where h_1 and h_2 are the metric coefficients for the η and ξ coordinates, respectively. The boundary conditions are as follows:

1) along the axis of symmetry ($\eta = 0$),

$$\frac{\partial\phi}{h_1\partial\eta} = 0$$

2) far away from the current source ($\eta = 1$), $\phi = \phi(r,z)$

3) far below the free surface ($\xi = 0$), $\phi = \phi(r,z)$

4) along the free surface ($\xi = 1$),

$$\frac{\sigma}{h_2}\frac{\partial\phi}{\partial\xi} = J_\xi$$

where J_ξ is the ξ-component of the current density vector $\vec{J}$.

Boundary condition 1) is the result of the requirement of zero current flux across

KEY WORDS

Electromagnetic Force
Induced Convection
Weld Pool Convection
Free Surface Pools
Gas Tungsten Arc Welding
Pool Surface Fitting
Heat Transfer
Fluid Flow
Sozou Analysis
Induced Magnetism

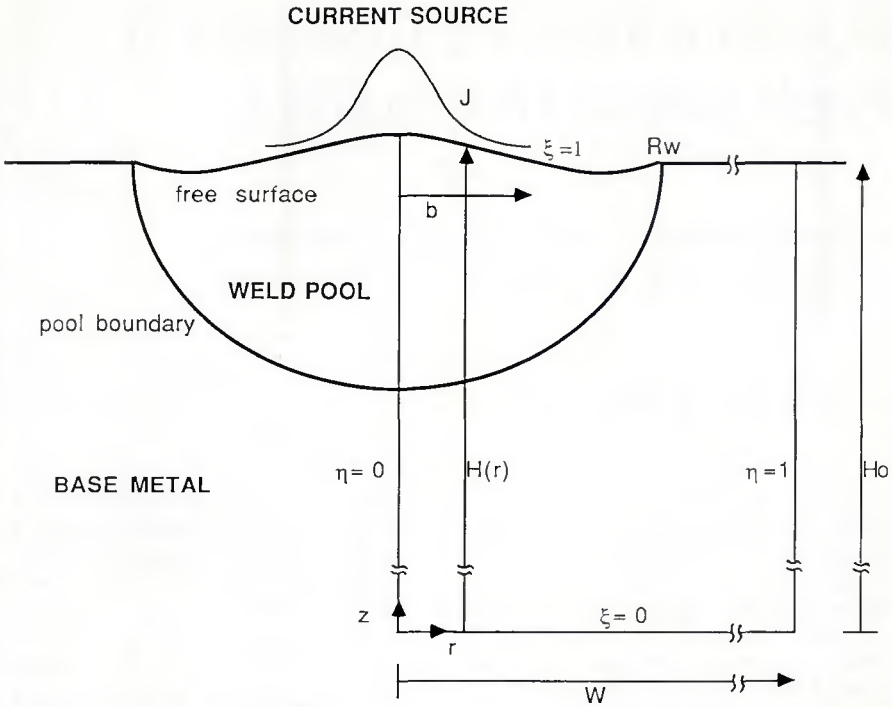

Fig. 1—Schematic sketch of the weld pool and the coordinates used for heat and fluid flow calculation.

the axis of symmetry. Boundary conditions 2) and 3) are based on the fact that far away from the current source, the effect of pool surface deformation is no longer significant and the analytical solution of Equation 3 is, therefore, valid. Referring to Fig. 1, we found W = 10 mm (0.4 in.) and H_o = 18 mm (0.7 in.) to be sufficient and further increases in these values resulted in no significant changes. Boundary condition 4) is the result of the requirement of zero tangential current flux along the free surface (and the top surface of the base metal, too). For a slightly deformed pool surface, J_ξ in boundary condition 4) can be approximated by the current density distribution described in Equation 1. For a significantly deformed pool surface, Equation 1 and the corresponding equation for the power density distribution to be shown later, are no longer valid, as pointed out by Lin, *et al.* (Ref. 25). Although our model here is valid for general pool surface deformations, Equation 1 will still be used here as an approximation in view of the slight pool surface deformations involved.

From the calculated potential field, the current density distribution in the weld pool can be obtained from Ohm's law as follows:

$$J_\eta = -\frac{\sigma}{h_1}\frac{\partial\phi}{\partial\eta} \tag{6}$$

$$J_\xi = -\frac{\sigma}{h_2}\frac{\partial\phi}{\partial\xi} \tag{7}$$

With the help of the Maxwell equations, the following equation can be obtained:

$$\frac{1}{rh_1}\frac{\partial}{\partial\eta}(rB_\theta) = \mu_o J_\xi \tag{8}$$

where B_θ and μ_o are the self-induced azimuthal magnetic flux and magnetic permeability, respectively. The other two components of the induced magnetic flux vector, *i.e.*, B_η and B_ξ, are zero. From Equation 8 and the boundary condition that $B_\theta = 0$ at $\eta = 0$,

$$B_\theta = \frac{1}{r}\int_o^\eta \mu_o r J_\xi h_1 d\eta \tag{9}$$

Equations 6 through 9 can be used to calculate the electromagnetic force $\vec{J}\times\vec{B}$ in the weld pool.

The equation of continuity is as follows:

$$\frac{\rho}{h_1h_2 r}\left[\frac{\partial}{\partial\eta}(h_2 ru) + \frac{\partial}{\partial\xi}(h_1 rw)\right] = 0 \tag{10}$$

where u and w are, respectively, the velocity components in the η and ξ directions, and ρ is the density.

The η and ξ components of the equation of motion are as follows (Ref. 26):

$$\frac{\rho}{h_1h_2 r}\left[\frac{\partial}{\partial\eta}(h_2 r u^2) + \frac{\partial}{\partial\xi}(h_1 r uw)\right] = -\frac{1}{h_1}\frac{\partial P}{\partial\eta} + \frac{1}{h_1h_2 r}\left[\frac{\partial}{\partial\eta}(h_2 r\sigma_{11}) + \frac{\partial}{\partial\xi}(h_1 r\sigma_{21})\right] + \frac{\sigma_{12}}{h_1h_2}\frac{\partial h_1}{\partial\xi} - \frac{\sigma_{22}}{h_1h_2}\frac{\partial h_2}{\partial\eta} + \frac{\rho w^2}{h_1h_2}\frac{\partial h_2}{\partial\eta} - \frac{\rho uw}{h_1h_2}\frac{\partial h_1}{\partial\xi} - \frac{\sigma_{33}}{h_1 r}\frac{\partial r}{\partial\eta} + \rho g_\eta - J_\xi B_\theta \tag{11}$$

$$\frac{\rho}{h_1h_2 r}\left[\frac{\partial}{\partial\eta}(h_2 r uw) + \frac{\partial}{\partial\xi}(h_1 r w^2)\right] = -\frac{1}{h_2}\frac{\partial P}{\partial\xi} + \frac{1}{h_1h_2 r}\left[\frac{\partial}{\partial\eta}(h_2 r\sigma_{12}) + \frac{\partial}{\partial\xi}(h_1 r\sigma_{22})\right] + \frac{\sigma_{21}}{h_1h_2}\frac{\partial h_2}{\partial\eta} - \frac{\sigma_{11}}{h_2h_1}\frac{\partial h_1}{\partial\xi} + \frac{\rho u^2}{h_1h_2}\frac{\partial h_1}{\partial\xi} - \frac{\rho uw}{h_1h_2}\frac{\partial h_2}{\partial\eta} - \frac{\sigma_{33}}{h_2 r}\frac{\partial r}{\partial\xi} + \rho g\xi + J_\eta B_\theta \tag{12}$$

where the components of the stress tensor $\sigma_{i,j}$ are as follows:

$$\sigma_{11} = 2\mu\left(\frac{1}{h_1}\frac{\partial u}{\partial\eta} + \frac{w}{h_1h_2}\frac{\partial h_1}{\partial\xi}\right)$$

$$\sigma_{22} = 2\mu\left(\frac{1}{h_2}\frac{\partial w}{\partial\xi} + \frac{u}{h_1h_2}\frac{\partial h_2}{\partial\eta}\right)$$

$$\sigma_{21} = \sigma_{12} = \mu\left[\frac{h_2}{h_1}\frac{\partial}{\partial\eta}\left(\frac{w}{h_2}\right) + \frac{h_1}{h_2}\frac{\partial}{\partial\xi}\left(\frac{u}{h_1}\right)\right]$$

$$\sigma_{33} = 2\mu\left(\frac{u}{h_1 r}\frac{\partial r}{\partial\eta} + \frac{w}{h_2 r}\frac{\partial r}{\partial\xi}\right.$$

g_η and g_ξ are the η and ξ components of the gravitational acceleration $\vec{g}$. The Boussinesq approximation (with the use of a thermal expansion coefficient β) is used to approximate the buoyancy force.

The equation of energy is as follows:

$$\frac{\rho}{h_1h_2 r}\left[\frac{\partial}{\partial\eta}(h_2 r uH) + \frac{\partial}{\partial\xi}(h_1 r wH)\right] = \frac{1}{h_1h_2 r}\left[\frac{\partial}{\partial\eta}\left(\frac{h_2 r}{h_1}k\frac{\partial T}{\partial\eta}\right) + \frac{\partial}{\partial\xi}\left(\frac{h_1 r}{h_2}k\frac{\partial T}{\partial\xi}\right)\right] \tag{13}$$

where H is the enthalpy, k the thermal conductivity and T the temperature. The use of the enthalpy H in Equation 13 allows the heat of fusion to be considered while the position of the pool boundary is being determined in the heat flow calculation, *i.e.*, the "enthalpy method."

The boundary conditions for fluid flow are as follows:

1) At the weld pool centerline ($\eta = 0$), $u = 0$ and $\sigma_{12} = 0$

2) At the free surface ($\xi = 1$) (Ref. 27),

$$w = 0$$

$$\sigma_{21} = 0$$

$$P_a + \sigma_{22} - P + C = -\gamma\left[\frac{h''}{(1+h'^2)^{3/2}} + \frac{h'}{r(1+h'^2)^{1/2}}\right] \text{ with}$$

$$h'(0) = h(R_w) = 0 \text{ and } h = H_o - H(r) \tag{14}$$

where σ_{21} is the shear stress, σ_{22} is the normal stress, P_a is the ambient pressure, P is the pressure from the equation of motion and h is the local weld pool depression. The values h″ and h′ are the second and first derivatives of h with respect to r, respectively. The constant C, which is a reference pressure, is determined from the following constraint of constant volume:

Table 1—Physical Properties of 6061 Aluminum Alloy (Ref. 5)

β	$= 1.0 \times 10^{-4}$ °C^{-1}	ρ	$= 2700$ kg/m^3
γ	$= 914 \times 10^{-3}$ N/m	C_s	$= 1066$ J/kg°C
T_L	$= 652$°C	C_L	$= 1066$ J/kg°C
T_S	$= 582$°C	k_S	$= 168$ watt/m°C
T_a	$= 25$°C	k_L	$= 108$ watt/m°C
ΔH	$= 3.95 \times 10^5$ J/kg	μ_L	$= 1.0 \times 10^{-3}$ kg/m s

$$2\pi \int_0^{R_w} rh\, dr = 0 \qquad (15)$$

where R_w is the radius of the weld pool surface.

3) At the weld pool boundary ($T = T_L$),

$u = w = 0$

The pool boundary is approximated by small steps of the finite-difference grid that are closest to the interface.

The boundary conditions for heat flow, on the other hand, are as follows:

1) At the weld pool centerline ($\eta = 0$),

$$\frac{1}{h_1}\frac{\partial T}{\partial \eta} = 0$$

2) At the free surface ($\xi = 1$),

$$-\frac{k}{h_2}\frac{\partial T}{\partial \xi} = \begin{cases} -\dfrac{3Q}{\pi a^2}\exp\left(\dfrac{-3r^2}{a^2}\right), & r \le a \\ h_c(T - T_a) + \sigma' e\,(T^4 - T_a^4), & r > a \end{cases}$$

where Q is the power delivered from the arc to the workpiece, a the effective radius of the arc, h_c the heat transfer coefficient, T_a the ambient temperature, σ' the Stefan-Boltzman constant, and e the emissivity. For aluminum alloys, the emissivity e ranges from 0.04 for shiny surfaces to 0.19 for heavily oxidized surfaces (Ref. 28), and the heat transfer coefficient h_c is approximately 8.5 W/m^2°C (Ref. 29). Due to the low melting point and high thermal conductivity of aluminum, the surface heat loss is usually small and can be neglected.

3) Far away from the centerline ($\eta = 1$), $T = T_1(z)$

4) Far below the free surface ($\xi = 0$), $T = T_o(r)$

$T_1(z)$ and $T_o(r)$ were obtained from the point-heat-source analytical solution of Rosenthal (Ref. 30). This solution, though less accurate near the location of the point heat source due to singularity, is in fact quite accurate in the region sufficiently far away from it. For the small heat input (1800 W) in a semi-infinite workpiece in the present investigation, we found W = 10 mm and H_o = 18 mm to be sufficient, as in the calculation of the potential field.

The method of solution is similar to that described in a previous study (Ref. 22) on pool surface deformation due to Marangoni convection, and hence, will not be repeated here. In brief, a finite volume method (*i.e.*, a volume-integral-type finite difference method) was employed and the SIMPLE algorithm (Ref. 31) was used to carry out computations in the physical domain, with the use of the hybrid scheme (Ref. 31) and weighted, rather than central, three-point differencing. Based on the normal stress balance at the weld pool surface, the shape of the surface was calculated from the velocity and temperature fields. A new grid system was then generated from the new surface shape for the calculation of the new electromagnetic force, velocity and temperature fields. This procedure was repeated until convergence was obtained.

Results and Discussion

Calculations were made for a stationary weld pool in 6061 aluminum alloy produced by gas tungsten arc welding at 150 A and 1800 W. The effective radii of the Gaussian current- and power-density distributions of this welding arc were 2 and 4 mm, respectively. The physical propeties of 6061 aluminum alloys are listed in Table 1. Although we recognize the effect of alloying elements on the surface tension of liquid aluminum, we still used the surface tension value of pure liquid aluminum (914×10^{-3} N/m) as an approximation, due to the lack of data.

Figure 2 shows a portion of the orthogonal grid mesh in its final form. As shown, the grid spacing is finer near the surface, centerline and edge of the weld pool, in order to enhance the accuracy of computation. It should be pointed out that the grid system is staggered, with components of the vector variables (*e.g.*, velocity, current density vector and magnetic field vector) being evaluated at midpoints of the line segments (representing the cell surfaces) and the scalar variables (*e.g.*, temperature and pressure) at the positions of the dots (representing the cell centers). The resultant vectors, however, are still plotted at the positions of the dots.

The calculated velocity field in the weld pool is shown in Fig. 3. In order to show the calculated velocity vectors more clearly, only a portion of the grid points was selected for plotting. Since the electromagnetic force in the weld pool acts inward and downward, the liquid metal flows radially inward along the pool surface and vertically downward along the centerline of the weld pool. The maximum velocity is about 0.4 m/s and is located about midway along the centerline of the weld pool.

In order to help explain the velocity field in Fig. 3, the current density and electromagnetic force fields are shown in Figs. 4 and 5, respectively. As shown in Fig. 4, the electric current converges toward the central area of the pool surface, as a result an inward and downward field of electromagnetic force is produced in the area, as shown in Fig. 5. This electromagnetic force field pushes the liquid metal in the area inward and downward, producing the velocity field shown in Fig. 3. It is interesting to note that the maximum electromagnetic force is located not at, but off the center of the pool surface. This is because $B_\theta = 0$ at the centerline ($\eta = 0$).

The calculated temperature field in the weld pool and shape of the weld pool surface are shown in Fig. 6. Due to the relatively high velocities of the vertically downward flow along the centerline of the weld pool, the portions of the 900°C

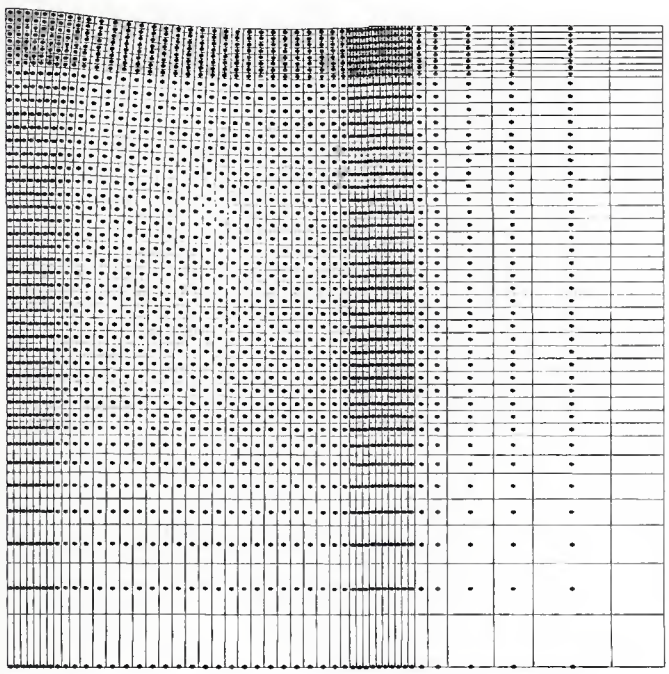

Fig. 2—A portion of the orthogonal curvilinear grid mesh used for computation.

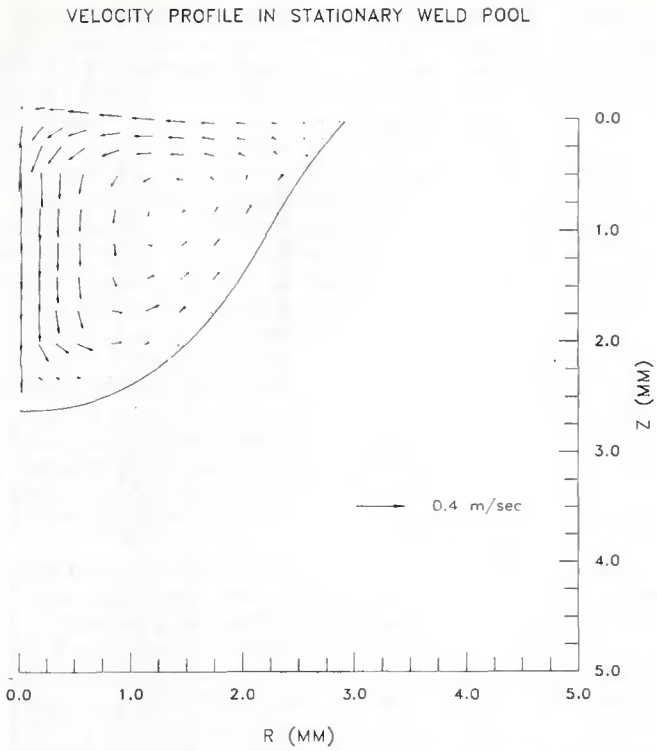

Fig. 3 — Calculated velocity field due to a Gaussian current source of 150 A.

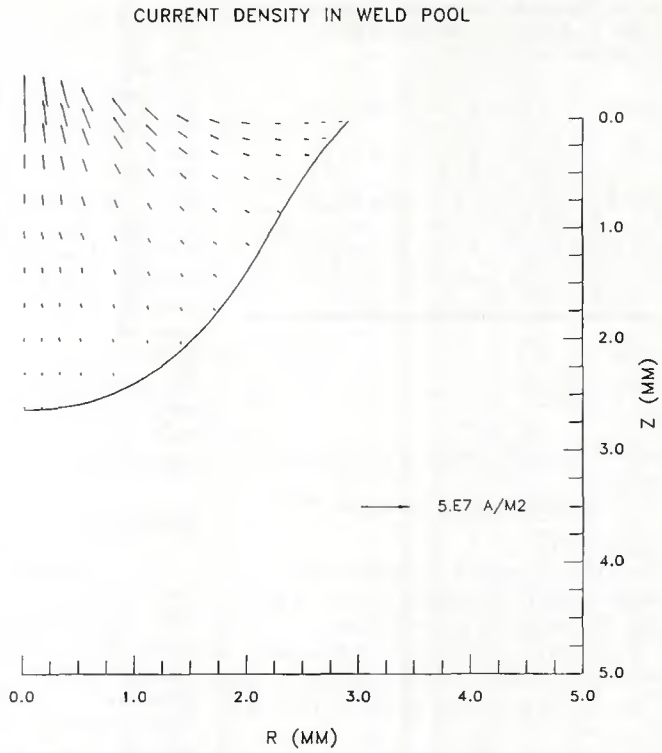

Fig. 4 — Calculated current-density field due to a Gaussian current source of 150 A.

(1652°F) and 1200°C (2192°F) isotherms adjacent to the centerline are pushed downward.

The calculated shape of the weld pool surface in Fig. 6 shows an elevation near the center and a very slight depression in the outer portion. Except at the edge of the weld pool, the liquid metal near the pool surface flows radially inward and is forced to deflect vertically downward near the centerline of the weld pool. As a result, the pool surface near the centerline of the weld pool is pushed upward and forms a small hump. The depression in the outer portion of the pool surface is rather small due to the larger radii in this portion of the pool surface.

The surface deformation due to the electromagnetic force in the weld pool described above, to the best of our knowledge, has not been reported previously. Although this phenomenon is interesting, it cannot possibly be verified experimentally, mainly due to the presence of other driving forces during welding. In this respect, computer modeling seems to be more informative.

According to the theoretical analysis of Sozou (Ref. 32), the center of the surface of a large pool should be depressed when it is subjected to a point current source of a small magnitude. This analysis, as subsequently pointed out by Andrews, *et al.* (Ref. 33), is valid for current levels lower than 0.5 A for steels and 0.63 A for aluminum. Since the surface deformation trend predicted by the analysis of Sozou for the point current source is opposite to what we have described above, it is essential for us to find out whether this discrepancy is merely due to differences in the nature of the current source or due to the inconsistency between the studies.

In order to do so, we made a calculation for a point current source of 0.3 A. This, however, presented two problems for us. First, a current source of 0.3 A for arc welding obviously does not even have enough power to produce a weld pool. In order to still have a weld pool for analysis, we chose to use a pool boundary identical to that for the weld pool shown in Fig. 6. Second, a current source of 0.3 A does not produce an electromagnetic

Fig. 5 — Calculated electromagnetic-force field due to a Gaussian current source of 150 A.

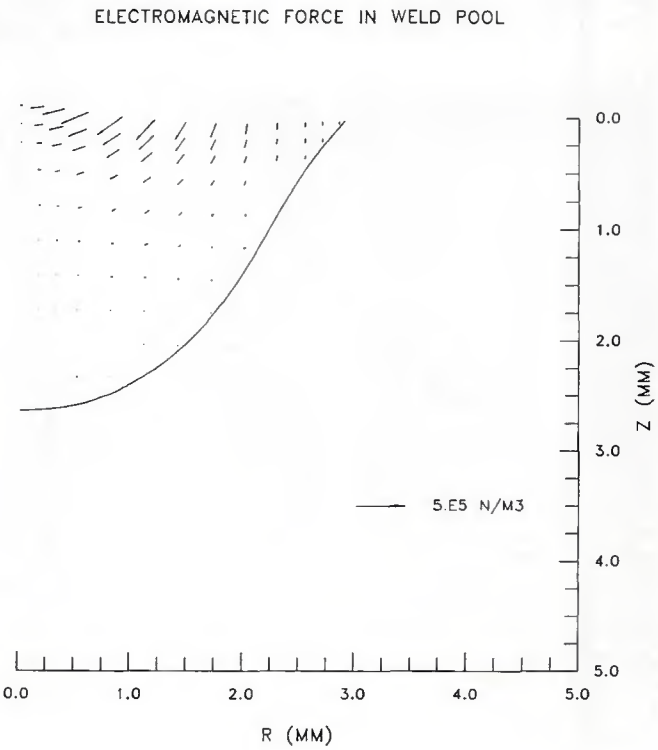

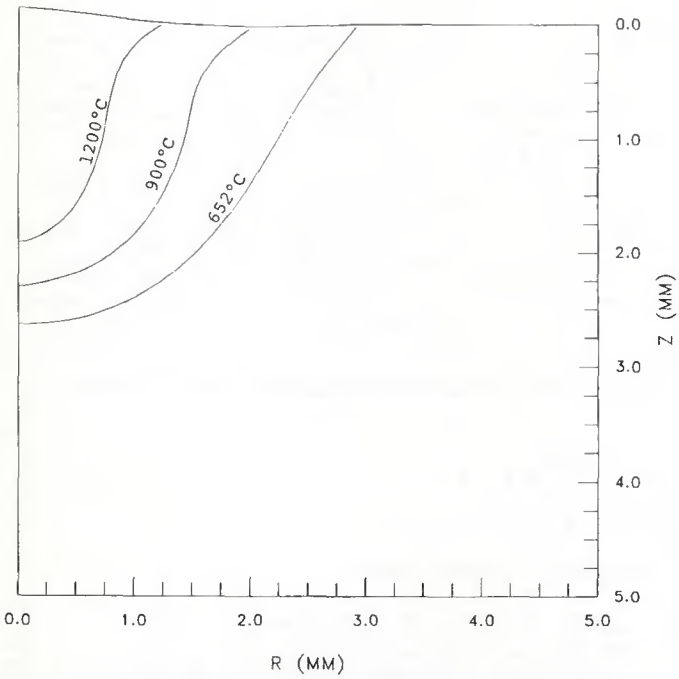

Fig. 6 — Calculated temperature field and shape of pool surface due to a Gaussian current source of 150 A. The center of the pool surface is elevated.

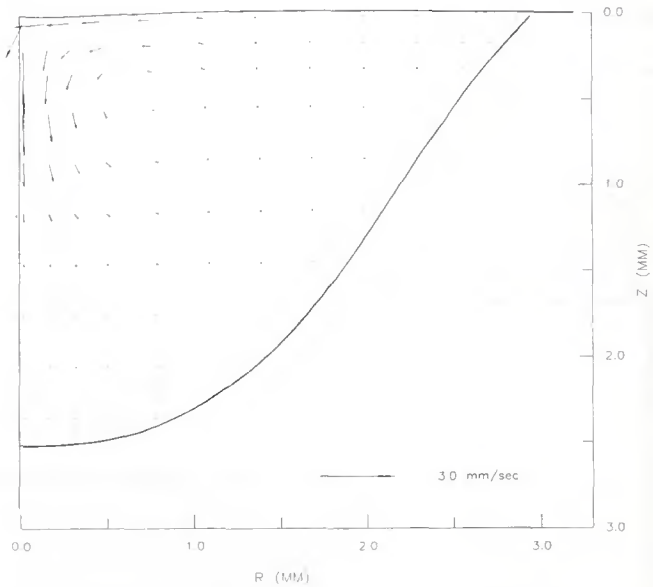

Fig. 7 — Calculated velocity field and shape of pool surface due to a point current source of 0.3 A. The center of the pool surface is very slightly depressed. Note that the pool boundary is specified in this case.

force large enough to cause any significant surface deformation in liquid metals, which have rather high surface tensions. In order to allow the surface deformation to be detectable, we decided to reduce the surface tension of molten aluminum by 10^4 times, and drop the buoyancy force.

Figure 7 shows the calculated velocity field in the weld pool and shape of the pool surface due to the 0.3-A point source. As shown, the electromagnetic-force-induced flow is similar to that shown in Fig. 3 for the previous case, being radially inward along the pool surface and vertically downward along the pool centerline. The maximum velocity is about 4 mm/s and is located along the centerline of the weld pool shortly below the surface. However, the flow is significant only in the vicinity of the point current source, and the extent of the radially inward flow is not great enough to cause the formation of a hump near the center of the pool surface. On the contrary, the downward pushing electromagnetic force produced by the point current source causes a slight depression near the center of the pool surface. Our model is, therefore, consistent with the theoretical analysis of Sozou (Ref. 32). It should be pointed out here that in Fig. 7, the radial components of the velocity vectors near the top of the weld pool centerline do not appear to be zero. This is because these velocity vectors are located at the positions of the dots, which are close to, but not exactly along the centerline of the weld pool, as can be seen from Fig. 2. Along the centerline of the weld pool, the radial components of the velocity vectors are exactly zero, as required by boundary condition 1 for fluid flow.

Finally, it should also be pointed out that in the study of Kublanov, *et al.* (Ref. 34), a gas jet was directed onto the center of the surface of a liquid metal pool to produce a local depression. This simulated the effect of the arc pressure, rather than the effect of the electromagnetic force in the weld pool, on pool surface deformation. In fact, no pool surface deformation due to the electromagnetic force in the weld pool was studied. As such, quoting the work of Kublanov, *et al.* (Ref. 34), as an evidence for the surface depression caused by the electromagnetic force in the weld pool, which Sozou (Ref. 32) did, is not exactly adequate.

Conclusions

1) The current density, the induced magnetic field and the resultant electromagnetic force were calculated in a weld pool with a deformed surface.

2) Electromagnetic-force-induced weld pool convection tends to cause an elevation near the center of the weld pool surface and a slight depression in its outer portion.

3) The calculated pool surface deformation due to a point current source is consistent with the theoretical analysis of Sozou.

Acknowledgments

The authors acknowledge the support for the study from the National Science Foundation under NSF Grant No. DMR 8419274.

References

1. Oreper, G. M., Eagar, T. W., and Szekely, J. 1983. *Welding Journal* 62(11):307-s to 313-s.
2. Oreper, G. M., and Szekely, J. 1984. *J. Fluid. Mech.*, Vol. 147, pp. 53–79.
3. Chan, C., Mazumder, J., and Chen, M. M. 1984. *Metall. Trans.* Vol. 15A, pp. 2175–2184.
4. Kou, S., and Sun, D. K. 1985. *Metall. Trans.* Vol. 16A, pp. 203–213.
5. Kou, S., and Wang, Y. H. 1986. *Welding Journal*, 65(3):63-s to 70-s.
6. Kou, S., and Wang, Y. H. 1986. *Metall. Trans.* Vol. 17A, pp. 2265–2270.
7. Kou, S., and Wang, Y. H. 1986. *Metall. Trans.* Vol. 17A, pp 2271–2277.
8. Wang, Y. H., and Kou, S. 1986. *Modeling and Control of Casting and Welding Processes*, S. Kou and R. Mehrabian, eds. The Metallurgical Society, Warrendale, Pa., pp. 197–210.
9. Correa, S. M., and Sundell, R. E *ibid*, pp. 221–227.
10. Chan, C. L., Zehr, R., Mazumder, J., and Chen, M. M. *ibid*, pp. 229–246.
11. Szekely, J., Oreper, G. M., and Mckelliget, J. *ibid*, pp. 247–276.
12. Szekely, J. 1986. *Advances in Welding Science and Technology*, S. A. David, ed. ASM International, Materials Park, Ohio, pp. 3–14.

13. Paul, A., and DebRoy, T. *ibid*, pp. 29–33.
14. Sundell, R. E., Solomon, H. D., and Correa, S. M. *ibid*, pp. 53–57.
15. Kanouff, M. P. 1987. *Numerical Methods in Thermal Problems*, Vol. V, Part 1, R. W. Lewis, K. Morgan and W. G. Habashi, eds. Pineridge Press, U.K., pp. 15–26.
16. Craine, R. E., 1987. *Applied Scientific Research*, 1987, Vol. 44, pp. 261–275.
17. Tsao, K. C., and Wu, C. S. 1988. *Welding Journal* 67(3):70-s to 75-s.
18. Zacharia, T., Eraslan, A. H., and Aidun, D. K. 1988. *Welding Journal* 67(1):18-s to 27-s.
19. Zacharia, T., Eraslan, A. H., and Aidun, D. K. 1988. *Welding Journal* 67(3):53-s to 62-s.
20. Paul, A., and DebRoy, T. *Modeling of Casting and Welding Processes*. The Metallurgical Society, Warrendale, Pa., in press.
21. McLay, R., and Carey, G. F. *Int. J. Num. Meth. in Fluids*. in press.
22. Tsai, M. C., and Kou, S. *ibid*.
23. Tsai, M. C., and Kou, S. *Modeling of Casting and Welding Processes*. The Metallurgical Society, Warrendale, Pa., in press.
24. Tsai, M. C., and Kou, S. 1988. unpublished work, University of Wisconsin, Madison, Wis.
25. Lin, M. L., and Eagar, T. W. 1986. *Advances in Welding Science and Technology*. S. A. David, ed., ASM International, Materials Park, Ohio, pp. 47–51.
26. Malvern, L. E. 1969. *Introduction to the Mechanics of a Continuous Medium*. Prentice-Hall, Inc., N.J., pp. 641–672.
27. Landau, L. D., and Lifshitz, E. M. 1987. *Fluid Mechanics*, 2nd ed., Pergamon Press, Oxford, U.K., p. 241.
28. Rohsenow, W. M., and Choi, M. Y. 1961. *Heat, Mass and Momentum Transfer*. Prentice Hall, N.Y., p. 523.
29. Schlinninger, D. E., Betz, I. G., and Markus, H. 1970. *Welding Journal* 49(9):410-s to 418-s.
30. Rosenthal, D. 1941. *Welding Journal* 20(5):220-s to 234-s.
31. Patankar, S. V. 1980. *Numerical Heat Transfer and Fluid Flow*. Hemisphere Publishing Corp., McGraw-Hill Book Co., N.Y. pp. 88 and 126.
32. Sozou, C., and Pickering, W. M. 1976. *J. Fluid Mech.* Vol. 73, pp. 641–650.
33. Andrews, J. G., and Craine, R. E. 1978. *J. Fluid Mech.* Vol. 84, pp. 281–290.
34. Kublanov, V., and Erokhin, A. *IIW Doc. 212-218-74*, International Institute of Welding, London, England.

WRC Bulletin 336
September 1988

Interpretive Report on Dynamic Analysis of Pressure Components—Fourth Edition

This fourth edition represents a major revision of WRC Bulletin 303 issued in 1985. It retains the three sections on pressure transients, fluid structure interaction and seismic analysis. Significant revisions were made to make them current. A new section has been included on Dynamic Stress Criteria which emphasizes the importance of this technology. A new section has also been included on Dynamic Restraints that primarily addresses snubbers, but also discusses alternatives to snubbers, such as limit stop devices and flexible steel plate energy absorbers.

Publication of this report was sponsored by the Subcommittee on Dynamic Analysis of Pressure Components of the Pressure Vessel Research Committee of the Welding Research Council. The price of WRC Bulletin 336 is $20.00 per copy, plus $5.00 for postage and handling. Orders should be sent with payment to the Welding Research Council, Suite 1301, 345 E. 47th St., New York, NY 10017.

WRC Bulletin 343
May 1989

Destructive Examination of PVRC Weld Specimens 202, 203 and 251J

This Bulletin contains three reports:

(1) Destructive Examination of PVRC Specimen 202 Weld Flaws by JPVRC
By Y. Saiga

(2) Destructive Examination of PVRC Nozzle Weld Specimen 203 Weld Flaws by JPVRC
By Y. Saiga

(3) Destructive Examination of PVRC Specimen 251J Weld Flaws
By S. Yukawa

The sectioning and examination of Specimens 202 and 203 were sponsored by the Nondestructive Examination Committee of the Japan Pressure Vessel Research Council. The destructive examination of Specimen 251J was performed at the General Electric Company in Schenectady, N.Y., under the sponsorship of the Subcommittee on Nondestructive Examination of Pressure Components of the Pressure Vessel Research Committee of the Welding Research Council. The price of WRC Bulletin 343 is $24.00 per copy, plus $5.00 for U.S., or $8.00 for overseas, postage and handling. Orders should be sent with payment to the Welding Research Council, Room 1301, 345 E. 47th St., New York, NY 10017.